In presenting the dissertation as a partial fulfillment of the requirements for an advanced degree from the Georgia Institute of Technology, I agree that the Library of the Institute shall make it available for inspection and circulation in accordance with its regulations governing materials of this type. I agree that permission to copy from, or to publish from, this dissertation may be granted by the professor under whose direction it was written, or, in his absence, by the Dean of the Graduate Division when such copying or publication is solely for scholarly purposes and does not involve potential financial gain. It is understood that any copying from, or publication of, this dissertation which involves potential financial gain will not be allowed without written permission.

7/25/68

THERMAL STRESSES IN TUBES AND CYLINDRICAL TANKS

A THESIS

Presented to

The Faculty of the Division of Graduate

Studies and Research

by

Harry E. Flanders, Jr.

In Partial Fulfillment

of the Requirements for the Degree

Master of Science in Mechanical Engineering

Georgia Institute of Technology

June, 1970

THERMAL STRESSES IN TUBES AND CYLINDRICAL TANKS

Approved:

Chairman

Date approved by Chairman: May 29, 1947

ACKNOWLEDGMENTS

As the author of this thesis I wish to express my thanks and appreciation to all who have contributed directly and indirectly in its preparation.

I am especially grateful to Dr. John H. Murphy for his encouragement and guidance during the investigation. Appreciation is also extended to Dr. William J. Lnenicka and Dr. W. Wulff for their helpful review of the work.

TABLE OF CONTENTS

LIST OF FIGURES

SUMMARY

The thermal stresses during transient and steady state heating of axially restrained, infinitely long tubes are examined in this thesis. The uncoupled thermoelastic equations of heat conduction and thermal stresses in polar coordinates are the governing equations, and they are solved by the use of a finite difference approximation. As a check of the accuracy of the numerical solution, the exact solution of steady state stress and temperature distributions were compared with that of the numerical calculation. The numerical accuracy was in error a maximum of 0.9 per cent which is a combination of truncation and round-off errors.

By the comparison of the maximum surface stresses for different conditions of thermal shock and steady state heating, it was found that a general statement can be made. For a heating condition with the Biot modulus of the heated surface equal to that of the non-heated, thermal shock always produces the largest stress on the heated surface, and the steady state condition always produces the largest stress on the non-heated surface. It can also be stated that as the Biot modulus of the non-heated surface changes, the value of the steady state stresses changes, but the thermal shock stresses do not. The thermal shock stresses do not change because the maximum stress occurs at the time when the non-heated surface just begins to change temperature; thus the Biot modulus of that surface could be any value and not change the result.

An approximate formulation of the ratio of thermal shock stresses in tubes over the thermal shock stresses in a flat plate was obtained by fitting a curve to the calculated data points. Thus by the use of Manson's[10] approximate equation of thermal shock stresses in a flat plate and the correction factor for the tube, the thermal shock stresses for a tube may be calculated.

GLOSSARY OF ABBREVIATIONS

Material Properties

E	modulus of elasticity (p.s.i.)
α	linear coefficient of thermal expansion (in/in/°F)
μ	Poisson's ratio
k	thermal conductivity (BTU/hr ft °F)
C	volumetric heat capacity (BTU/ft^3 °F)
D	thermal diffusivity (ft^2/hr) [=k/C]

Variables

r	radial coordinate in polar coordinate system (inches)
θ	circumferential coordinate in polar coordinate system (radians)
$\bar{d}$	mean tube diameter (inches)
w	tube wall thickness (inches)
t	time (seconds)
T	temperature (°F)
u	radial displacement (inches)
ϵ	normal strain (in/in)
$\bar{e}$	truncation error
σ_{rr}	radial stress (lb/in^2)
$\sigma_{\theta\theta}$	tangential stress (lb/in^2)
σ^*	nondimensional stress $\left[= \frac{(1-\mu)\sigma}{E\alpha\Delta T}\right]$
ϕ	Airy stress function

h	coefficient of heat transfer (BTU/hr ft^2 °F)
N_{Bi}	Biot modulus [=hw/k]
N_{Fo}	Fourier number [=Dt/w^2]

Subscripts

r	radial
θ	tangential
I	inside
O	outside
i	spatial increment
j	time increment

Prefix

Δ	small increment

CHAPTER I

INTRODUCTION

In many engineering designs involving tubes and tanks the temperature will vary throughout the wall thickness. Such temperature gradients produce stresses which must be superimposed on the stresses of the applied structural loads. In many cases these "thermal stresses" are of great importance and must be considered in detail.

To calculate the "thermal stresses," the temperature distribution through the wall must be known. In cases of steady state heating, the stresses can be calculated by a closed form solution.[14] For the condition of transient heating, the temperature distribution and stresses cannot be calculated by a closed-form solution; thus either a series solution or finite difference solution must be used. A finite difference method for the solution of the temperature distribution, as well as the stress distribution, was used in this thesis.

Since the higher thermal gradients are produced during the transient period of heating up or cooling down, the problem of "thermal shock" is of importance. When thermal stress is generated by sudden changes in temperature, the process is referred to as "thermal shock."[10] For higher heating and cooling rates these transient stresses peak up much higher than the steady state stresses.

A typical temperature and stress distribution for a thermal shock condition is shown in Figure 1. This is an inside heating condition

with a transient temperature distribution which produces a maximum tangential stress at the inside surface. The radial stresses produced are generally small relative to the tangential stresses and are always zero at the surfaces. For the long tube, plane strain analysis, the axial stress and tangential stress are equal at the surface. For the investigation of this thesis, the maximum value of tangential stress will be the major point of concern. It was observed that for thermal shock, the maximum value of tangential stress occurred at the surface on which heating was applied. If the tube is cooled in lieu of heated, the maximum stresses occur on the same respective surfaces as for heating.

In this thesis the main concern is the presentation of thermal stresses in a useful form so that the engineer can evaluate the thermal stresses and determine their relative importance in his particular structural application. The results will be presented in a form such that the stresses given by Manson's flat plate equation[10] can be modified to produce the stresses in a tube. The Manson equation relates the maximum thermal stress reached on the surface of a flat plate to the Biot modulus, N_{Bi}, and is given by

$$\frac{1}{\sigma^*_{max}} = 1.5 + \frac{3.25}{N_{Bi}} - 0.5e^{-16/N_{Bi}}$$

Chapter II gives the fundamental equations governing the analysis of thermal shock of tubes as well as the boundary conditions. Chapter III presents the numerical analysis of the governing equations and discusses the accuracy of the numerical solution. Chapter IV gives the

solution of thermal shock stresses for conditions of inside as well as outside heating and a discussion of the results. Chapter V presents the modification of Manson's[10] equation to account for the wall curvature.

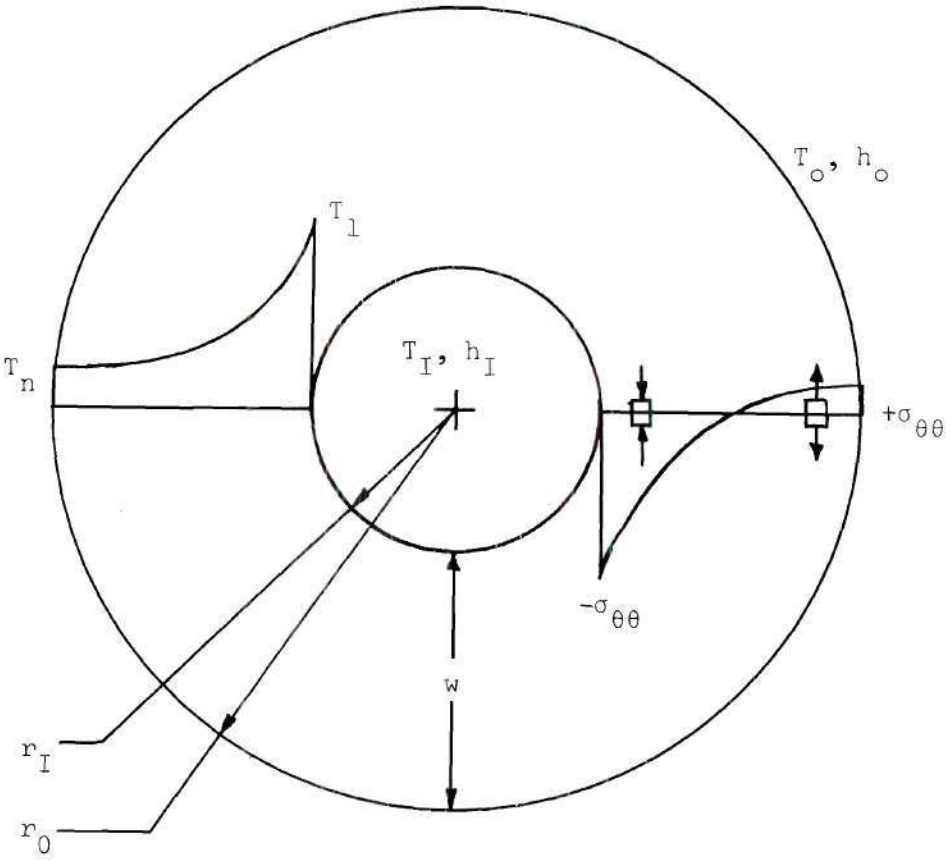

Figure 1. Typical Transient Temperature and Stress Distribution for Inside Heating

CHAPTER II

DEVELOPMENT OF GOVERNING EQUATIONS

The basic equations of thermoelasticity are such that temperature and stress are interrelated. The exact solution of the general thermoelasticity problem is difficult to obtain, but fortunately in most applications it is possible to omit the mechanical coupling term in the energy equation and the inertia term in the equation of motion without significant error. With these assumptions the theory is referred to as "uncoupled quasistatic-theory," and the problem is changed into a heat conduction problem and a thermal stress problem.

As shown in Appendix B, the use of the uncoupled equations does not produce a significant error in problems with Biot moduli in the range of 0.1 through 20.0; thus the uncoupled equations were used.

Heat Conduction Equation

The heat conduction equation in polar coordinates for the case of no axial and no tangential heat conduction as shown in Appendix B is

$$\frac{\partial^2 T}{\partial r^2} + \frac{1}{r}\frac{\partial T}{\partial r} = \frac{1}{D}\frac{\partial T}{\partial t} \tag{1}$$

The solution of this equation is obtained through the application of initial condition and boundary conditions. The initial condition is that the temperature distribution is known at time equal zero.

$$\text{For } r_I \leq r \leq r_O \qquad T_r = T_{initial} \tag{2}$$

The boundary conditions are that the tube is assumed to be heated (or cooled) by convection at both its inside and outside surfaces. This condition is expressed by

$$\text{For } r = r_I \qquad -k \frac{\partial T}{\partial r} = h(T_{fluid} - T_{surface})$$

$$\text{For } r = r_O \qquad -k \frac{\partial T}{\partial h} = h(T_{surface} - T_{fluid}) \tag{3}$$

Stress Equations

The problem of thermal stresses in a long tube with a radial temperature distribution, without externally applied forces, and without body forces is a plane strain problem and is solved by the use of isotropic elasticity relations.

The radial temperature distribution is symmetrical with respect to the centerline of the tube, and independent of the axial coordinate. Since the temperature does not vary with θ, the stresses do not vary with θ. Thus the equilibrium equation for axial symmetric stress is[14]

$$\frac{\partial \sigma_{rr}}{\partial r} + \frac{\sigma_{rr} - \sigma_{\theta\theta}}{r} = 0 \tag{4}$$

For the thermal stress problem with no externally applied forces, the radial stress at the inside surface and outside surface will be zero. Thus the two boundary conditions are

$$\begin{aligned} &\text{At} \quad r = r_I && \sigma_{rr} = 0 \\ &\text{At} \quad r = r_O && \sigma_{rr} = 0 \end{aligned} \tag{5}$$

The compatibility equation will be developed with the use of the stress-strain and strain-displacement equations. The thermal stress-strain equations[14] in polar coordinates are

$$\begin{aligned} \epsilon_{rr} &= \frac{1}{E}[\sigma_{rr} - \mu(\sigma_{\theta\theta}+\sigma_{zz})] + \alpha T \\ \epsilon_{\theta\theta} &= \frac{1}{E}[\sigma_{\theta\theta} - \mu(\sigma_{rr}+\sigma_{zz})] + \alpha T \\ \epsilon_{zz} &= \frac{1}{E}[\sigma_{zz} - \mu(\sigma_{rr}+\sigma_{\theta\theta})] + \alpha T \end{aligned} \tag{6}$$

For plane strain analysis, axially restrained, $\epsilon_{zz} = 0$, and the third of Equations 6 reduces to

$$\sigma_{zz} = \mu(\sigma_{rr}+\sigma_{\theta\theta}) - E\alpha T \tag{7}$$

Substituting Equation 7 into Equations 6 yields the stress-strain equations in polar coordinates.

$$\epsilon_{rr} = \frac{(1-\mu^2)}{E}\left(\sigma_{rr} - \frac{\mu}{1-\mu}\sigma_{\theta\theta}\right) + (1+\mu)\alpha T$$

$$\epsilon_{\theta\theta} = \frac{(1-\mu^2)}{E}\left(\sigma_{\theta\theta} - \frac{\mu}{1-\mu}\sigma_{rr}\right) + (1+\mu)\alpha T \qquad (8)$$

The strain displacement equations in polar coordinates for a plane strain analysis of axial symmetry[14] are

$$\epsilon_{rr} = \frac{du}{dr}$$

$$\epsilon_{\theta\theta} = \frac{u}{r} \qquad (9)$$

In Equations 8 and 9 there are four equations and five unknowns. Since Equations 9 are expressed in terms of one unknown, u, the relation between them will be found. By differentiating the second of Equations 9 with respect to (r) and substituting the result into the first of Equations 9 the relation is found.

$$\epsilon_{rr} = \epsilon_{\theta\theta} + r\frac{d\epsilon_{\theta\theta}}{dr} \qquad (10)$$

By differentiating the second of Equations 8 with respect to (r) and substituting this value and the values of Equations 8 into Equation 9, the compatibility equation for a plane strain, axially symmetric problem is obtained.

$$\frac{(1-\mu)}{E}\frac{d\sigma_{\theta\theta}}{dr} - \frac{\mu}{E}\frac{d\sigma_{rr}}{dr} - \frac{1}{rE}(\sigma_{rr}-\sigma_{\theta\theta}) = -\frac{d(\alpha T)}{dr} \tag{11}$$

Thus with the equilibrium equation, Equation 4, the compatibility equation, Equation 11, and the boundary conditions, Equation 5, and the temperature distribution, the solution may be obtained. In this thesis the solution will be obtained by the use of the Airy stress function.

The stresses in terms of the Airy stress function[7] in polar coordinates are

$$\sigma_{rr} = \frac{1}{r}\frac{\partial\phi}{\partial r} + \frac{1}{r^2}\frac{\partial^2\phi}{\partial\theta^2}$$
$$\sigma_{\theta\theta} = \frac{\partial^2\phi}{\partial r^2} \tag{12}$$

Since the stresses do not vary with θ, the second derivative of the stress function, ϕ, will be zero, and the first of Equations 12 reduces to

$$\sigma_{rr} = \frac{1}{r}\frac{\partial\phi}{\partial r} \tag{13}$$

By substituting the values of the Airy stress function, Equations 12 and 13, into the equilibrium equation, Equation 4, it is seen that the equilibrium equation is identically satisfied.

Substituting the values of the Airy stress function, Equations 12 and 13, into the compatibility equation, Equation 11, yields the compatibility equation in terms of the Airy stress function. Since the

Airy stress function is a function of (r) only, the partial derivative is changed to an ordinary derivative.

$$\frac{d^3\phi}{dr^3} + \frac{1}{r}\frac{d^2\phi}{dr^2} - \frac{1}{r^2}\frac{d\phi}{dr} = -\frac{E}{(1-\mu)}\frac{d(\alpha T)}{dr} \tag{14}$$

The solution of the stresses can be obtained by solving Equation 14. This equation is a third order differential equation which requires three boundary conditions in the solution. We have two boundary conditions involving the stresses, Equations 5. Since the stresses are not dependent on the absolute value of the Airy stress function, the third boundary condition is obtained by an arbitrary choice of the value of the stress function at one point. The three boundary conditions are

$$\frac{d\phi}{dr} = 0 \quad \text{and} \quad \phi = 0 \quad \text{at } r = r_I$$

$$\frac{d\phi}{dr} = 0 \quad \text{at } r = r_O \tag{15}$$

CHAPTER III

NUMERICAL ANALYSIS

For the solution of the stress compatibility equation, Equation 12, the use of the Airy stress function was decided upon. The solution using the Airy stress function can be obtained, with a high degree of accuracy, by the use of a finite difference numerical analysis. Since the stress compatibility equation was solved by a finite difference analysis, it was decided that the heat conduction equation, Equation 14, would be solved by a finite difference analysis.

When finite difference equations are used, the question of accuracy[12] of the finite difference approximation must be considered. Numerical solutions involve several types of errors. One of these errors is "round-off error," which is defined as the difference between the exact solution to the finite difference equation and the numerical values calculated. A second kind of error, "truncation error," is defined as the difference between the exact solution and the exact finite difference solution. In problems involving a time increment as well as a spatial increment, the way numerical errors grow or decay with time is a problem having to do with the "stability" of the finite difference equations. A certain relationship between the time increment and spatial increment must be maintained to insure that the numerical error does not grow with time. When this relationship is maintained, the solution is said to be "stable." As the "truncation error" is

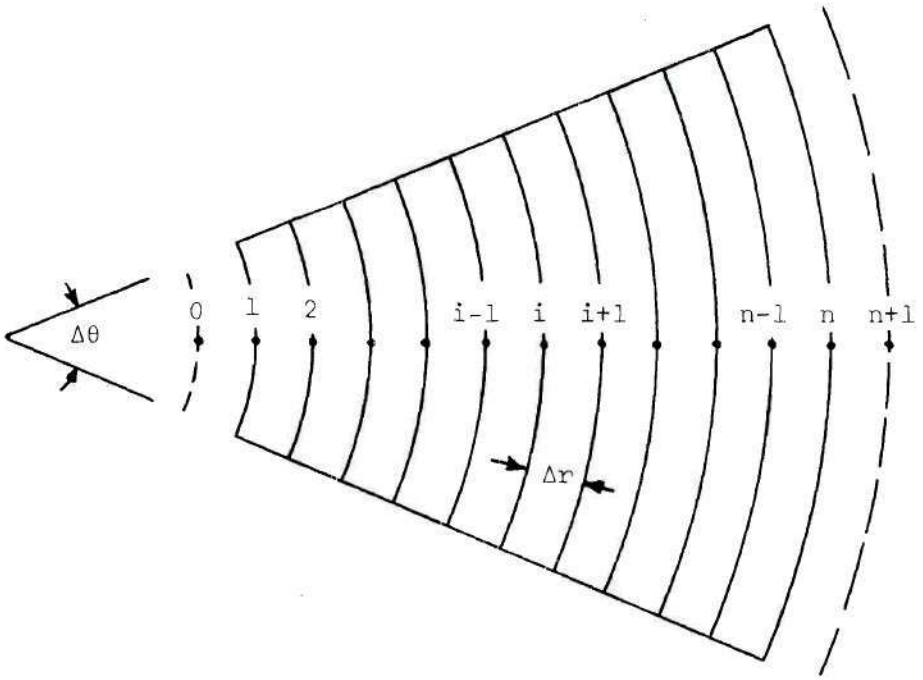

Figure 2. Finite Difference Grid

reduced by choosing smaller subdivisions providing "stability" is maintained and the derivatives of higher orders are continuous and bounded, the solution approaches the corresponding value of the differential equation. This is defined as "convergence."

In the following sections, the finite difference approximation for the temperature and stress equations will be developed. Attention will be given to the problems of "truncation error," "convergence," "stability" and "round-off error."

To formulate the finite difference equations, the tube is cut into the elemental form shown in Figure 2.

Finite Difference Formulation of the Heat Conduction Equation

To develop the heat conduction equation, Equation 1, in finite difference formulation, the Taylor's series is used. The expansion of the Taylor's series with respect of radius, subscript (i), and time, subscript (j), is as follows.

$$T_{i+1,j} = T_{i,j} + \Delta r \left.\frac{\partial T}{\partial r}\right|_{i,j} + \frac{(\Delta r)^2}{2!} \left.\frac{\partial^2 T}{\partial r^2}\right|_{i,j} + \frac{(\Delta r)^3}{3!} \left.\frac{\partial^3 T}{\partial r^3}\right|_{i,j} + \cdots \quad (16)$$

$$T_{i-1,j} = T_{i,j} - \Delta r \left.\frac{\partial T}{\partial r}\right|_{i,j} + \frac{(\Delta r)^2}{2!} \left.\frac{\partial^2 T}{\partial r^2}\right|_{i,j} - \frac{(\Delta r)^3}{3!} \left.\frac{\partial^3 T}{\partial r^3}\right|_{i,j} + \cdots \quad (17)$$

$$T_{i,j+1} = T_{i,j} + \Delta t \left.\frac{\partial T}{\partial t}\right|_{i,j} + \frac{(\Delta t)^2}{2!} \left.\frac{\partial^2 T}{\partial t^2}\right|_{i,j} + \cdots \quad (18)$$

Subtracting Equation 18 from Equation 17 yields the first derivative with respect to (i).

$$\left.\frac{\partial T}{\partial r}\right|_{i,j} = \frac{T_{i+1,j} - T_{i-1,j}}{2\Delta r} - \frac{(\Delta r)^2}{6}\left.\frac{\partial^3 T}{\partial r^3}\right|_{i,j} + \cdots \qquad (19)$$

Adding Equation 17 and Equation 18 yields the second derivative with respect to (i).

$$\left.\frac{\partial^2 T}{\partial r^2}\right|_{i,j} = \frac{T_{i+1,j} - 2T_{i,j} + T_{i-1,j}}{\Delta r^2} - \frac{\Delta r^2}{12}\left.\frac{\partial^4 T}{\partial r^4}\right|_{i,j} + \cdots \qquad (20)$$

Rearranging Equation 16 yields the first derivative with respect to (j).

$$\left.\frac{\partial T}{\partial t}\right|_{i,j} = \frac{T_{i,j+1} - T_{i,j}}{\Delta t} - \frac{\Delta t}{2}\left.\frac{\partial^2 T}{\partial t^2}\right|_{i,j} + \cdots \qquad (21)$$

Substituting these derivatives, Equations 19, 20, and 21, into the heat conduction equation, Equation 14, yields the finite difference equation for the temperature.

$$\frac{T_{i+1,j} - 2T_{i,j} + T_{i-1,j}}{\Delta r^2} - \frac{\Delta r^2}{12}\left.\frac{\partial^4 T}{\partial r^4}\right|_{i,j} + \frac{1}{r_i}\left[\frac{T_{i+1,j} - T_{i-1,j}}{2\Delta r} - \frac{\Delta r^2}{6}\left.\frac{\partial^3 T}{\partial r^3}\right|_{i,j}\right]$$

$$- \frac{1}{D}\left[\frac{T_{i,j+1} - T_{i,j}}{\Delta t} - \frac{\Delta t}{2}\left.\frac{\partial^2 T}{\partial r^2}\right|_{i,j}\right] = 0$$

Solving for the temperature at the advanced time interval and excluding the terms involving $(\Delta r)^2$ and (Δt) produces the explicit equation of temperature.

$$T_{i,j+1} = \left(1 - \frac{2D\Delta t}{\Delta r^2}\right)T_{i,j} + \left(\frac{D\Delta t}{\Delta r^2} + \frac{D\Delta t}{2r_i \Delta r}\right)T_{i+1,j} + \left(\frac{D\Delta t}{\Delta r^2} - \frac{D\Delta t}{2r_i \Delta r}\right)T_{i-1,j} \qquad (22)$$

The terms involving $(\Delta r)^2$ and (Δt) that were neglected are the truncation error which is written as

$$\bar{e} = 0\{(\Delta r)^2\} + 0\{\Delta t\}$$

Thus the truncation error is of the order of $(\Delta r)^2$ and (Δt).

Another point of concern is the way in which the error accumulates as the time interval increases in this type of problem. The solution will remain stable provided the coefficients of the finite difference equation are all positive.[2] To maintain positive coefficients in Equation 22 the following limits must be maintained.

$$\frac{D\Delta t}{\Delta r^2} \leq \frac{1}{2}$$

$$\Delta r \leq 2r_i \qquad (23)$$

By satisfying Equation 23 with the proper ratic of Δr and Δt the explicit solution of the temperature at the interior nodal points will

produce a stable solution and will converge to the exact solution as Δr and Δt approach zero.

The boundary conditions must be examined. To develop the finite difference formulation at the boundary the heat balance at the surface, Equation 3, is used at the inside surface. To obtain the first partial derivative of temperature with respect to radius at nodal point (1), the Taylor's series is developed for temperatures at nodal points (2) and (3).

$$T_{2,j+1} = T_{1,j+1} + \Delta r \left.\frac{\partial T}{\partial r}\right|_{1,j+1} + \frac{\Delta r^2}{2!} \left.\frac{\partial^2 T}{\partial r^2}\right|_{1,j+1} + \cdots$$

$$T_{3,j+1} = T_{1,j+1} + (2\Delta r) \left.\frac{\partial T}{\partial r}\right|_{1,j+1} + \frac{(2\Delta r)^2}{2!} \left.\frac{\partial^2 T}{\partial r^2}\right|_{1,j+1} + \cdots \qquad (24)$$

The first derivative is obtained by multiplying the second of Equations 24 by four and subtracting the first of Equations 24 from the result. Thus the first partial derivative with the truncation error is

$$\left.\frac{\partial T}{\partial r}\right|_{1,j+1} = \frac{-3T_{1,j+1} + 4T_{2,j+1} - T_{3,j+1}}{2\Delta r} - \frac{\Delta r^2}{3} \left.\frac{\partial^3 T}{\partial r^3}\right|_{1,j+1} \qquad (25)$$

Substituting Equation 25 into Equation 3 and solving for the temperature at nodal point (1) and excluding the truncation error term, yields the explicit difference equation for the temperature at nodal point (1).

$$T_{1,j+1} = \frac{1}{3k + 2h\Delta r} (2h\Delta r T_I + 4kT_{2,j+1} - kT_{3,j+1}) \qquad (26)$$

The truncation error is

$$\bar{e} = 0\{(\Delta r)^2\}$$

Thus the boundary condition produces the same "truncation error" as the interior nodal points.

By expressing this finite difference equation at the advanced time interval, the temperature at the surface nodal point is calculated from the temperatures of the two adjacent interior nodal points at this advanced time and the temperature of ambient fluid. This scheme eliminates the time variable in the finite difference equation. By the use of vonNeumann's[12] condition for stability it can be shown that the "variational" equation is independent of the time-dependent portion of the error term. Thus the error cannot grow with time, and the boundary equation, Equation 26, is stable provided the interior nodal points are stable. Thus as Δr approaches zero the solution converges to the exact solution of the differential equation, Equation 3.

The boundary condition for the outside surface, nodal point (n), is basically the same as the inside surface, thus possesses the same accuracy and stability as the inside surface.

Finite Difference Formulation of the Stress Compatibility Equation

The finite difference formulation of the stress compatibility equation, Equation 14, for a general interior nodal point (i) (see Figure 2) is obtained by expanding the Taylor's series for the nodal points as given below.

$$\phi_{i+2} = \phi_i + (2\Delta r)\left.\frac{d\phi}{dr}\right|_i + \left.\frac{(2\Delta r)^2}{2!}\frac{d^2\phi}{dr^2}\right|_i + \cdots \tag{27}$$

$$\phi_{i+1} = \phi_i + \Delta r\left.\frac{d\phi}{dr}\right|_i + \left.\frac{\Delta r^2}{2!}\frac{d^2\phi}{dr^2}\right|_i + \cdots \tag{28}$$

$$\phi_{i-1} = \phi_i - \Delta r\left.\frac{d\phi}{dr}\right|_i + \left.\frac{\Delta r^2}{2!}\frac{d^2\phi}{dr^2}\right|_i + \cdots \tag{29}$$

$$\phi_{i-2} = \phi_i - 2\Delta r\left.\frac{d\phi}{dr}\right|_i + \left.\frac{(2\Delta r)^2}{2!}\frac{d^2\phi}{dr^2}\right|_i + \cdots \tag{30}$$

The finite difference formulation of the first derivative with respect to (r) is found by subtracting Equation 29 from 28. Thus the first derivative with the error is

$$\left.\frac{d\phi}{dr}\right|_i = \frac{\phi_{i+1} - \phi_{i-1}}{2\Delta r} - \left.\frac{\Delta r^2}{6}\frac{d^3\phi}{dr^3}\right|_i + \cdots \tag{31}$$

The finite difference formulation of the second derivative is found by adding Equations 28 and 29. The second derivative is shown below with the error.

$$\left.\frac{d^2\phi}{dr^2}\right|_i = \frac{\phi_{i+1} - 2\phi_i + \phi_{i-1}}{\Delta r^2} - \left.\frac{\Delta r^2}{6}\frac{d^4\phi}{dr^3}\right|_i + \cdots \tag{32}$$

The finite difference formulation of the third derivative is found by substituting Equations 27, 28, 29, and 30 into the equation below.

$$(\text{Eq. } 27) - 2(\text{Eq. } 28) + 2(\text{Eq. } 29) - (\text{Eq. } 30) = 0$$

Thus the third derivative with the truncation error is

$$\left.\frac{d^3\phi}{dr^3}\right|_i = \frac{\phi_{i+2} - 2\phi_{i+1} + 2\phi_{i-1} - \phi_{i-2}}{2\Delta r^3} - \frac{\Delta r^2}{4}\left.\frac{d^5\phi}{dr^5}\right|_i + \cdots \qquad (33)$$

The finite difference formulation of the first derivative of temperature with respect to (r) is given by Equation 19. Substituting these derivatives, Equations 31, 32, 33, and 19 into the equation of compatibility, Equation 14, yields the finite difference formulation with truncation error. After collecting like terms, the following notation will be used to express the equation.

$$A_i = -r_i^2$$

$$B_i = 2r_i^2 + 2r_i\Delta r + \Delta r^2 \qquad (34)$$

$$C_i = -4r_i\Delta r$$

$$D_i = -2r_i^2 + 2r;\Delta r - \Delta r^2$$

$$E_i = r_i^2 \qquad (34)$$

$$F_i = -\frac{Er_i^2\Delta r^2\alpha(T_{i+1}-T_{i-1})}{(1-\mu)}$$

With the use of Equations 34 and neglecting the truncation term, the implicit finite difference formulation of the compatibility equation, applicable to the interior nodal points, is

$$A_i\phi_{i-2} + B_i\phi_{i-1} + C_i\phi_i + D_i\phi_{i+1} + E_i\phi_{i+2} = F_i \qquad (35)$$

$$i = 3,4,\cdots,n-2$$

Where the truncation error is

$$\bar{e} = 0\{(\Delta r)^2\}$$

As Δr approaches zero the finite difference formulation, Equation 35, converges in the limit to the exact value of the differential equation of compatibility, Equation 14.

As seen in Equation 41, the application of the finite difference equation involves five adjacent nodal points, and the application at every nodal point in the range introduces four external fictitious nodal points, two at each boundary. For the evaluation of these four points we have only three boundary conditions, Equation 13. Therefore to reduce the number of external nodal points,[4] a backward difference equation is used at the outside surface, nodal point (n). The derivatives are obtained by expanding the Taylor's series for the stress function at nodal points (n-1), (n-2), (n-3) and (n-4) and the temperature at the nodal points (n-1) and (n-2). By proper algebraic manipulation of the stress functions and temperatures, the derivatives can be obtained.

The first derivative is

$$\left.\frac{d\phi}{dr}\right|_n = \frac{3\phi_n - 4\phi_{n-1} + \phi_{n-2}}{2\Delta r} + \frac{\Delta r^2}{3}\left.\frac{d^3\phi}{dr^3}\right|_n \tag{36}$$

The second derivative is

$$\left.\frac{d^2\phi}{dr^2}\right|_n = \frac{2\phi_n - 5\phi_{n-1} + 4\phi_{n-2} - \phi_{n-3}}{\Delta r^2} + \frac{11}{12}\Delta r^2\left.\frac{d^4\phi}{dr^4}\right|_n \tag{37}$$

The third derivative is

$$\left.\frac{d^3\phi}{dr^3}\right|_n = \frac{5\phi_n - 18\phi_{n-1} + 24\phi_{n-2} - 14\phi_{n-3} + 3\phi_{n-4}}{2\Delta r^3} + \frac{7}{4}\Delta r^2\left.\frac{d^5\phi}{dr^5}\right|_n \tag{38}$$

The first derivative of temperature is

$$\left.\frac{dT}{dr}\right|_n = \frac{3T_n - 4T_{n-1} + T_{n-2}}{2\Delta r} + \frac{\Delta r^2}{3}\left.\frac{d^3T}{dr^3}\right|_n \tag{39}$$

Substituting these derivatives, Equations 36, 37, 38, and 39 into Equation 14 produces the implicit finite difference equation at nodal point (n). After collecting like terms, the notation can be simplified by setting

$$A_n = 3r_n^2$$

$$B_n = -14r_n^2 - 2r_n\Delta r$$

$$C_n = 24r_n^2 + 8r_n\Delta r + \Delta r^2 \qquad (40)$$

$$D_n = -18r_n^2 - 10r_n\Delta r + 4\Delta r^2 \qquad (40)$$

$$E_n = 5r_n^2 + 4r_n\Delta r - 3\Delta r^2$$

$$F_n = -\frac{Er_n^2\Delta r^2\alpha(3T_n - 4T_{n-1} + T_{n-2})}{(1-\mu)}$$

With the use of Equations 40 and neglecting the truncation error term, the finite difference equation at nodal point (n) is

$$A_n\phi_{n-4} + B_n\phi_{n-3} + C_n\phi_{n-2} + D_n\phi_{n-1} + E_n\phi_n = F_n \qquad (41)$$

where the truncation error is

$$\bar{e} = 0\{(\Delta r)^2\}$$

With the truncation error of the order of $(\Delta r)^2$, the finite difference formulation, Equation 41, converges to the exact solution of the differential equation as Δr approaches zero.

The boundary conditions for the finite difference equations are obtained from Equations 15. The first boundary condition is

$$\phi_1 = 0 \tag{42}$$

Referring to Figure 2, the second boundary condition is

$$\phi_0 = \phi_2$$

with a truncation error of

$$\bar{e} = 0\{(\Delta r)^2\}$$

Applying this boundary condition to Equation 41, at nodal point (2) produces the equation which eliminates the inside surface fictitious external nodal point (0).

$$B_2\phi_1 + (C_2+A_2)\phi_2 + D_2\phi_3 + E_2\phi_4 = F_2 \tag{43}$$

The third boundary condition is

$$\phi_{n+1} = \phi_{n-1}$$

with a truncation error of

$$\bar{e} = 0\{(\Delta r)^2\}$$

Applying this boundary condition to Equation 41 at nodal point (n-1)

produces the equation which eliminates the outside surface fictitious external nodal point (n+1).

$$A_{n-1}\phi_{n-3} + B_{n-1}\phi_{n-2} + (C_{n-1}+E_{n-1})\phi_{n-1} + D_{n-1}\phi_n = F_{n-1} \tag{44}$$

A solution to finite difference formulation of the compatibility equation can be obtained by writing Equation 35 at nodal points (3) through (n-2), using Equation 42 at nodal point (1), using Equation 43 at nodal point (2), using Equation 44 at nodal point (n-1), and using Equation 41 at nodal point (n). This produces a system of (n) linearly independent equations with (n) unknowns. The solution was obtained by placing the equations in augmented matrix form and reducing the matrix by the computer program presented in the Appendix.

The calculation of stresses from the stress function is accomplished by the use of Equation 10 and 11 in finite difference formulations. Neglecting the terms involving Δr^2 the finite difference formulation of the radial stress is

$$\sigma_{rr} = \frac{1}{r_i} \frac{\phi_{i+1} - \phi_{i-1}}{2\Delta r} \tag{45}$$

with a truncation error of

$$\bar{e} = 0\{(\Delta r)^2\}$$

The tangential stress is

$$\sigma_{\theta\theta} = \frac{\phi_{i+1} - 2\phi_i + \phi_{i-1}}{\Delta r^2} \tag{46}$$

with a truncation error of

$$\bar{e} = 0\{(\Delta r)^2\}$$

Accuracy of Numerical Solution

As a check of the numerical accuracy, the temperature distribution and stress distribution at the steady state condition were calculated for the smallest size tube investigated in this thesis and is shown in Figure 3. The numerical results were obtained by proceeding in time until the change in temperature was not greater than 0.005 per cent, and the stress was calculated from this temperature distribution. The exact solutions for the temperature and stress distributions were obtained from the closed form solutions given by Equations 47 and 48 in Chapter IV. The maximum difference between the exact and numerical solution for the temperature calculation is less than 0.1 per cent. The maximum difference between the exact and numerical solutions for the tangential stress calculation is 0.9 per cent.

For the calculations of this thesis the number of nodal points was 20 and the ratio of $(D\Delta t/\Delta r^2)$ was maintained at (1/6). This satisfied the limits for stability and produced a small grid. The small grid reduces the truncation error, but increases the number of calculations. To decrease the round-off error the temperature and stress function calculations were performed in double precision. Double

precision calculations use 16 decimal places instead of the normal 8 decimal places.

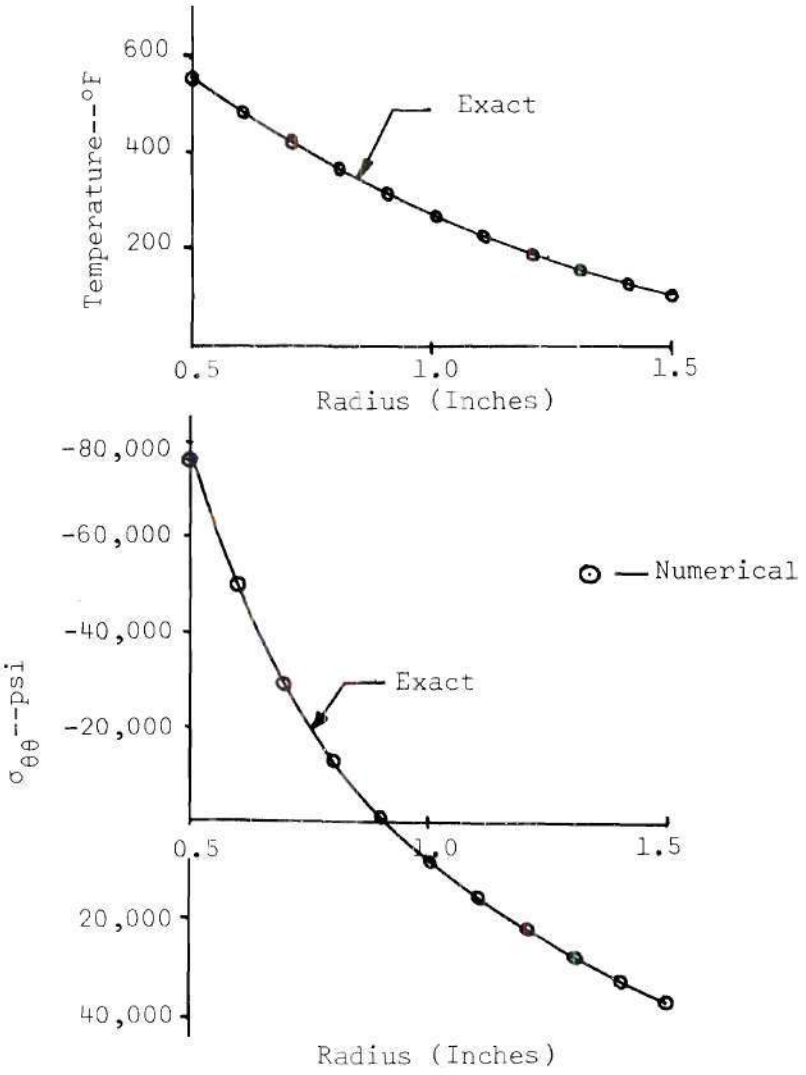

Figure 3. Steady State Temperature and Stress Distribution for $w/\bar{d} = 0.5$, $N_{Bi_I} = N_{Bi_O} = 20.0$, $T_I = 600°F$ and $T_o = 100°F$

CHAPTER IV

SOLUTION

This chapter presents the thermal stress distribution in tubes with temperature independent material properties. Different size tubes are investigated for transient heating as well as steady state heating. For the transient heating, different Biot moduli are used on the inside surface or outside surface while the Biot modulus on the opposite surface is equal to zero. The steady state heating is for different ratios of inside to outside Biot moduli.

Since the material properties are taken to be independent of temperature, the stresses are presented in nondimensional form involving the material constants. By the use of this data the maximum stress, either transient or steady state, may be evaluated in terms of the material constants and Biot modulus.

The temperature distribution, being a function of time, is evaluated at different time intervals. The stresses calculated from these temperature distributions are plotted as a function of time, and the time history of stress may be seen. From these stress-time plots the maximum stress can be obtained.

In order to present the stresses, four nondimensional parameters are used. These parameters are σ^*, N_{Bi}, N_{Fo} and $(w/\bar{d})$ (see Appendix B), and they present the stresses, heating, material properties, tube size

and time in nondimensional form. The first of the parameters is nondimensional stress.[10]

$$\sigma^* = \frac{\sigma(1-\mu)}{E\alpha\Delta T}$$

Where ΔT is defined as the difference between the ambient temperature and the uniform initial temperature of the tube. The physical interpretation of σ^* is the ratio of stress actually developed to the stress that would be developed if thermal expansion were completely constrained. The second parameter is the Biot modulus.

$$N_{Bi} = \frac{hw}{k}$$

The third parameter is the Fourier number.

$$N_{Fo} = \frac{Dt}{w^2}$$

The fourth parameter is nondimensional tube size, defined as the wall thickness divided by the mean tube diameter, $(w/\bar{d})$.

Thermal Shock Stresses

The transient heating of tubes on either the inside or outside surface, with a Biot modulus of zero on the opposite side, always produces a maximum stress which decreases to zero in the steady state condition. When heating tubes from the inside, the maximum compressive tangential stress occurs on the inside surface, while outside heating

produces a maximum on the outside surface. When cooling the tubes, the maximum tangential stresses occur on the same respective surfaces, but are tensile stresses instead of compressive stresses.

The tubes investigated in this thesis ranged from $(w/\bar{d})$ ratios of 0.5 to 0.1 which will cover most ordinary sizes of tubes used in structural applications. The range of Biot moduli investigated is from 0.1 to 20.

Inside Heating

To illustrate the peaking of the stresses, the nondimensional tangential stress at the inside surface and outside surface is plotted against Fourier number for a tube size, $(w/\bar{d})$, of 0.5. These plots, Figures 4 and 5, show the different maximum stresses reached for various Biot moduli.

Figure 6 shows that for the same Biot modulus, the maximum stress increases as the $(w/\bar{d})$ ratio increases. It can also be seen that as the $(w/\bar{d})$ ratio decreases, simulating large thin wall tubes, the maximum stress approaches that calculated by Manson[10] for the flat plate. Figure 6 also shows that the ratio of outside stress over inside stress for inside heating is low. Thus the stresses on the inside surface are of much greater importance.

Outside Heating

The peaking of the surface stresses for outside heating is illustrated by Figures 7 and 8 for a tube size, $(w/\bar{d})$, of 0.5. These stress-time plots are similar to the stress-time plots for the inside heating condition.

Figure 9 is the plot of the maximum nondimensional stresses on the outside surface for different size tubes and different Biot moduli. This figure illustrates that the maximum stress decreases as the $(w/\bar{d})$ ratio increases. Again it can be seen that as the $(w/\bar{d})$ ratio decreases, the maximum stresses approach that calculated by Manson[10] for the flat plate. From Figure 9 it can also be seen that the ratio of inside stress over outside stress for an outside heating condition is small, thus predicting that the stress on the outside surface for outside is of greater importance.

Steady State Stresses

The temperature[8] and stress[14] distributions for steady state heating or cooling conditions can be calculated from an exact solution. The steady state temperature difference between the inside surface and outside surface as a function of heating and material constants is

$$T_1 - T_n = \frac{(T_I - T_o)\ell n(r_o/r_I)}{\frac{k}{h_I r_I} + \ell n(r_o/r_I) + \frac{k}{h_o r_o}} \tag{47}$$

The steady state tangential stress as a function of the radius, temperature difference, and material constants is

$$\sigma_{\theta\theta} = \frac{E\alpha(T_1 - T_n)}{2(1-\mu)\ell n(r_o/r_I)} \left[1 - \ell n\left(\frac{r_o}{r_I}\right) - \frac{r_I^2}{r_o^2 - r_I^2}\left(1 + \frac{r_o^2}{r^2}\right) n\left(\frac{r_o}{r_I}\right) \right] \tag{48}$$

The condition of steady state inside heating and outside heating were

investigated for different ratios of the Biot modulus of the heated surface over the Biot modulus of the opposite surface. Figures 10, 11, 12, and 13 demonstrate the relationship between the steady state stresses and Biot moduli.

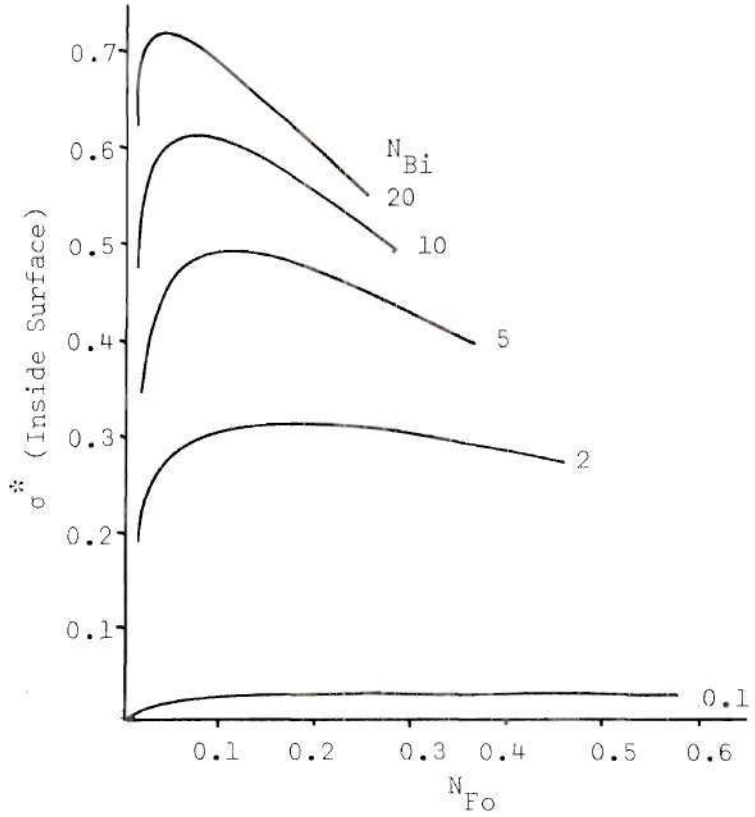

Figure 4. Nondimensional Stress versus Fourier Number for Inside Heating of Tube Size ($w/\bar{d}$ = 0.5)

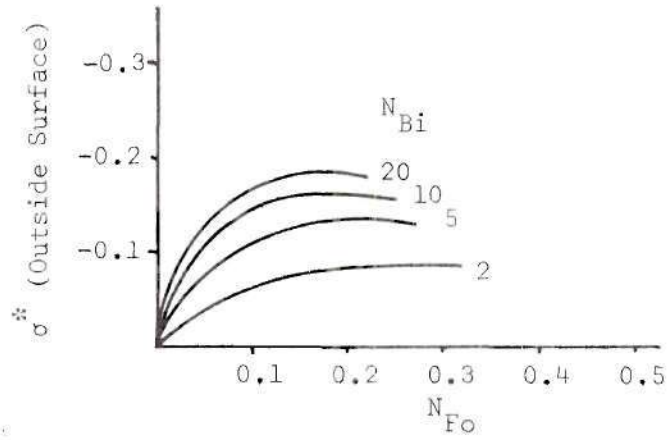

Figure 5. Nondimensional Stress versus Fourier Number for Inside Heating of Tube Size ($w/\bar{d}$ = 0.5)

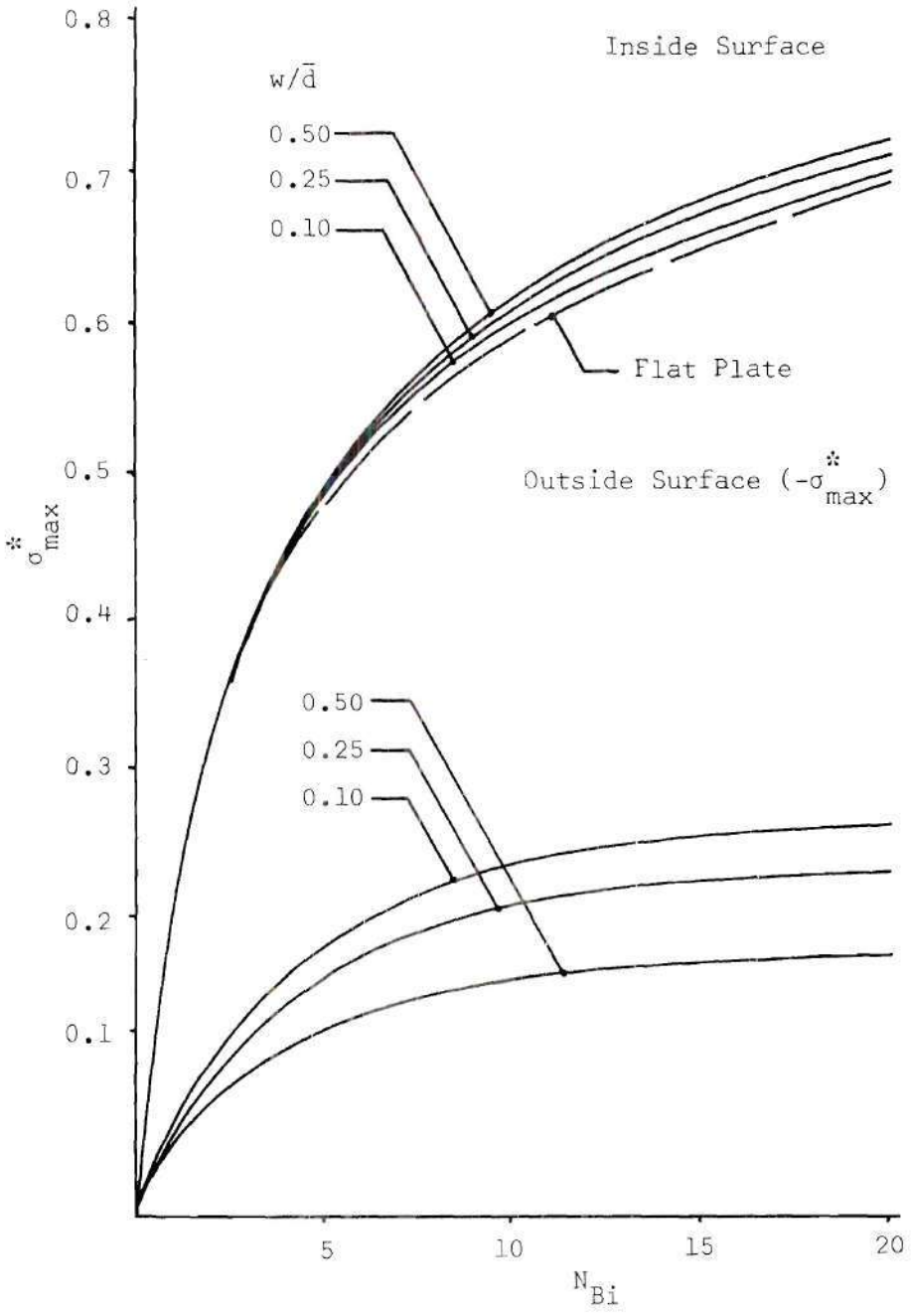

Figure 6. Maximum Nondimensional Stress versus Biot Modulus for Inside Thermal Shock

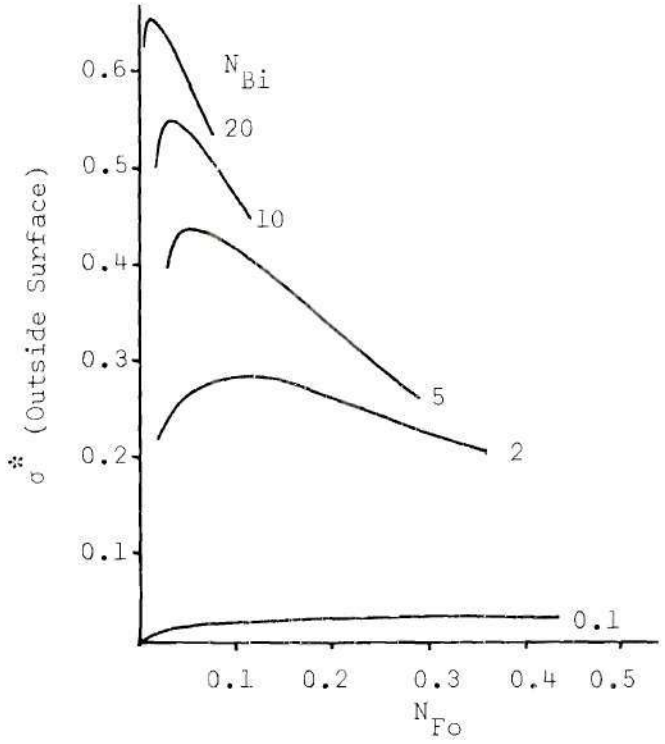

Figure 7. Nondimensional Stress versus Fourier Number for Outside Heating of Tube Size ($w/\bar{d}$ = 0.5)

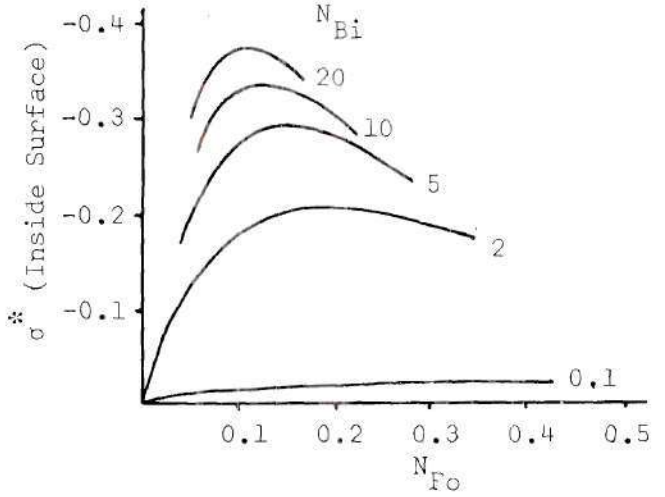

Figure 8. Nondimensional Stress versus Fourier Number for Outside Heating of Tube Size ($w/\bar{d}$ = 0.5)

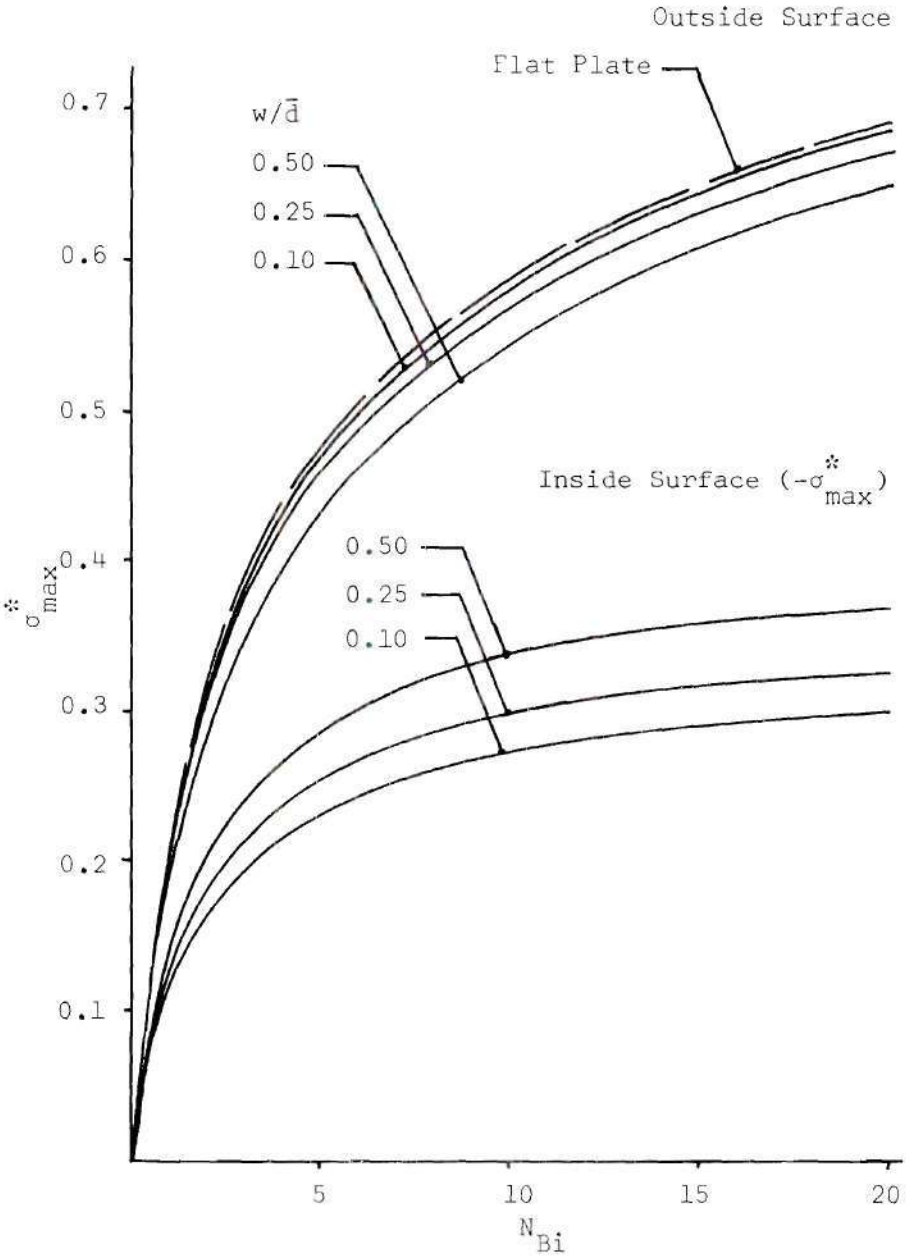

Figure 9. Maximum Nondimensional Stress versus Biot Modulus for Outside Thermal Shock

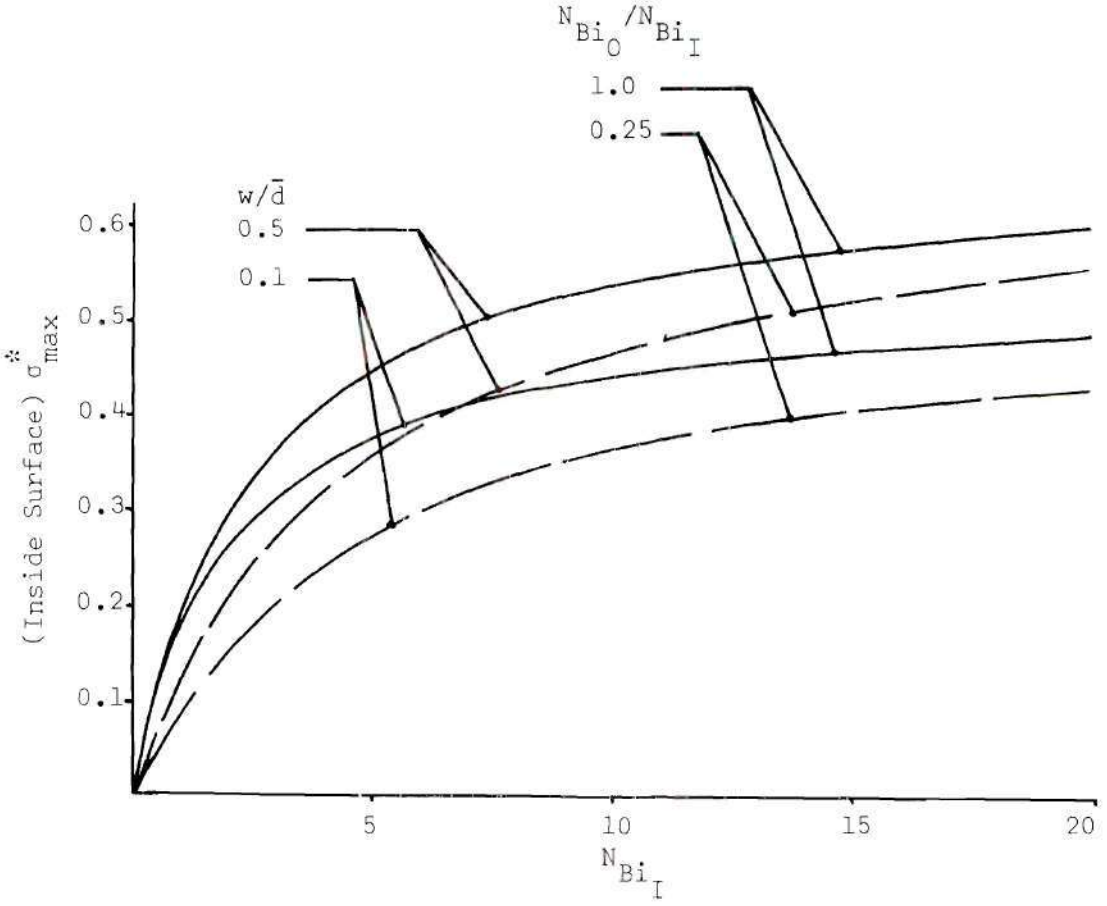

Figure 10. Maximum Nondimensional Stress versus Biot Modulus for Steady State Inside Heating

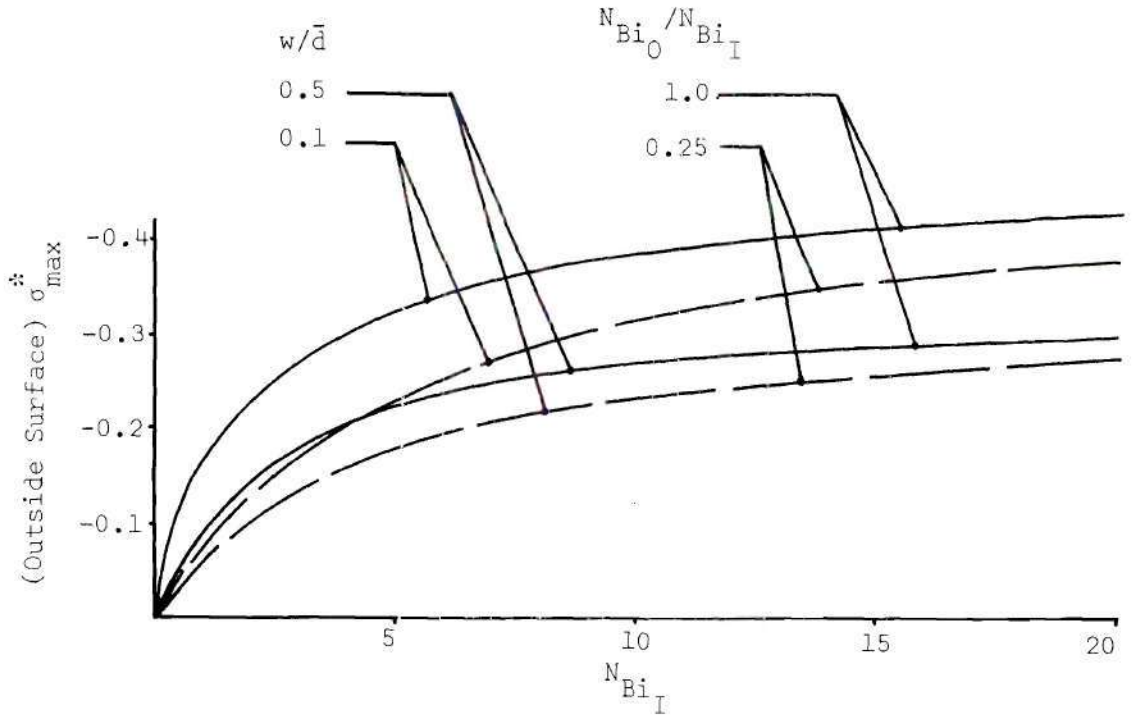

Figure 11. Maximum Nondimensional Stress versus Biot Modulus for Steady State Inside Heating

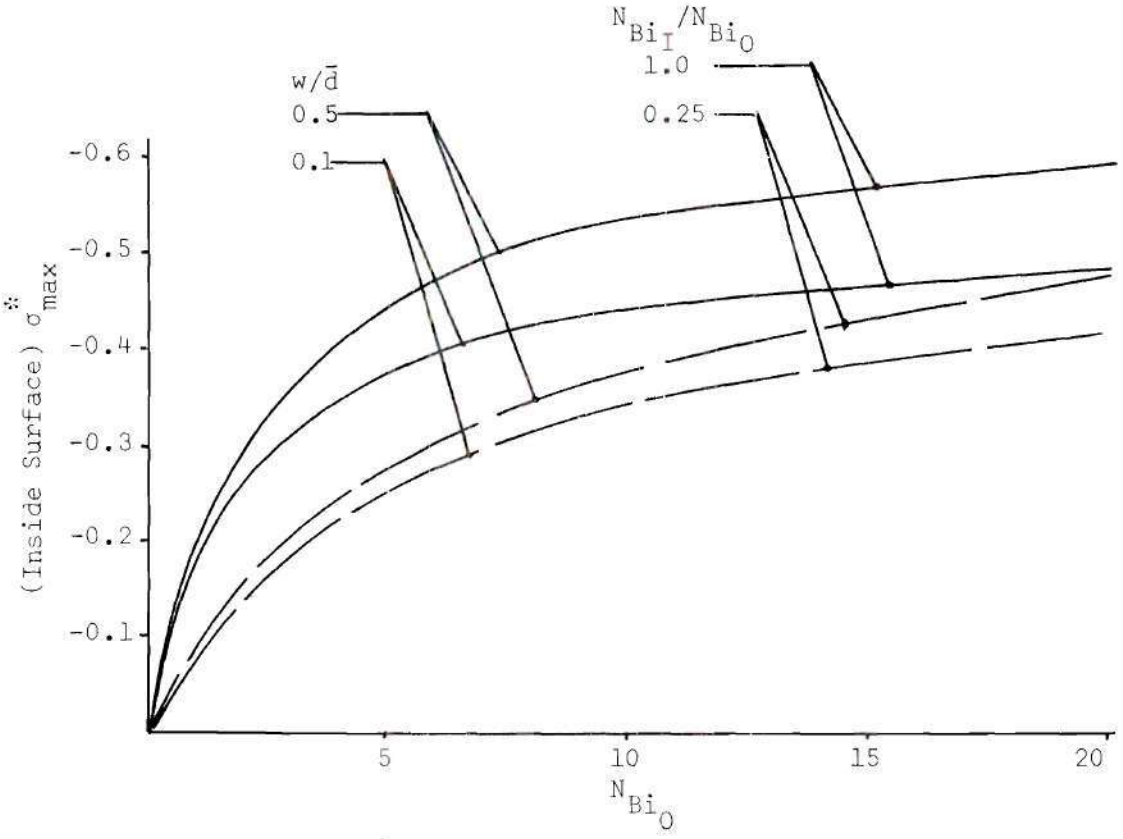

Figure 12. Maximum Nondimensional Stress versus Biot Modulus for Steady State Outside Heating

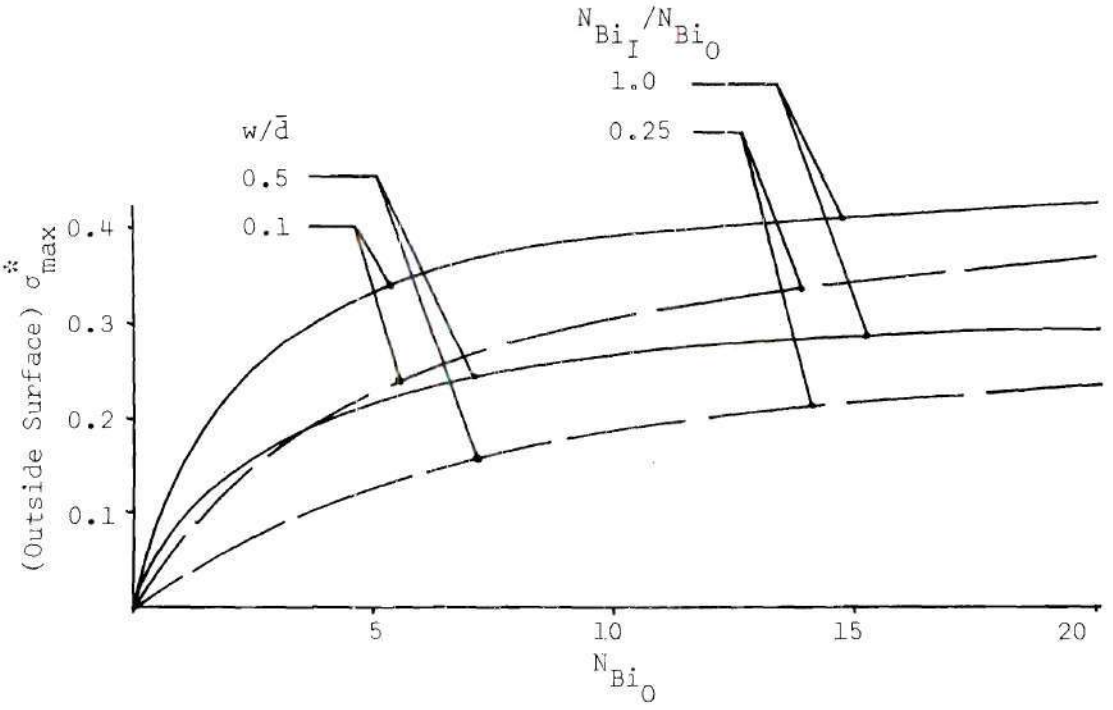

Figure 13. Maximum Nondimensional Stress versus Biot Modulus for Steady State Outside Heating

CHAPTER V

DISCUSSION OF RESULTS

The evaluation of the maximum stress developed during transient heating, by the use of a mathematical formulation, would be an aid to the engineer. Manson[10] developed an approximate mathematical formulation for the problem of thermal shock stresses of a flat plate.

$$\frac{1}{\sigma^*_{max}} = 1.5 + \frac{3.25}{N_{Bi}} - 0.5e^{-16/N_{Bi}} \tag{49}$$

From the data presented in Figures 6, 7, 10 and 11, it can be seen that as the $(w/\bar{d})$ ratio approaches zero the maximum stress approaches that of the flat plate. Thus a correction factor was developed which calculates stresses in tubes during thermal shock from the stresses in the flat plate during thermal shock.

Inside Heating Correction

The maximum stress on the inside surface for inside heating was examined at different Biot moduli for different size tubes. It can be seen from Figure 14 that the Biot modulus affected the correction by 20 per cent, but the correction is no larger than 4 per cent. Thus the ratio of maximum stress in the tube over maximum stress in the flat plate for inside heating was a function of the $(w/\bar{d})$ ratio only. The correction to Equation 49 for the calculation of maximum thermal shock

stress on the inside surface of a tube for inside heating is

$$\frac{\sigma^*_{max\ \text{Tube}}}{\sigma^*_{max\ \text{Flat Plate}}} = 1.0565 - 0.0190\ \ell n[1/(w/\bar{d})] \qquad (50)$$

This correction factor was obtained by fitting a curve to the data points shown in Figure 14 and is valid only in the range of $(w/\bar{d})$ of 0.08 through 0.5. For tubes with $(w/\bar{d})$ less than 0.08, the solution given by the flat plate equation will be accurate within 1.0 per cent. The solution given by this correction factor is accurate within 0.5 per cent for the range of $(w/\bar{d})$ of 0.08 through 0.5. For heating rates in the range of Biot moduli from 4 through 14, Manson's equation, Equation 49, has a maximum error of 1.7 per cent. Thus the overall error of the approximate formulation is in the range of 2.2 per cent.

Outside Heating Correction

The plot of the ratio of maximum stress in the tube over maximum stress in the flat plate versus $(w/\bar{d})$ ratio, Figure 15, is a family of curves with the Biot modulus as a parameter. Thus the correction to Equation 49 for the calculation of maximum thermal shock stress on the outside surface for outside heating is a function of the Biot modulus and the tube size, $(w/\bar{d})$ ratio. For a Biot modulus of 5 the correction factor is

$$\frac{\sigma^*_{max\ \text{Tube}}}{\sigma^*_{max\ \text{Flat Plate}}} = 1.0 - 0.188(w/\bar{d}) \qquad (51)$$

For a Biot modulus of 10 the correction factor is

$$\frac{\sigma^*_{max\ \text{Tube}}}{\sigma^*_{max\ \text{Flat Plate}}} = 1.0 - 0.150(w/\bar{d}) \qquad (51)$$

For a Biot modulus of 20 the correction factor is

$$\frac{\sigma^*_{max\ \text{Tube}}}{\sigma^*_{max\ \text{Flat Plate}}} = 1.0 - 0.122(w/\bar{d}) \qquad (51)$$

These correction factors were obtained by fitting a curve to the data points of Figure 15 and have a maximum error of 0.1 per cent. The overall error of the correction factor, Equation 51, and Manson's equation, Equation 49, is 1.8 per cent.

Comparison of Maximum Stresses

For the conditions of thermal shock and steady state heating, the maximum stress occurs on either the inside or outside surface for the different conditions.

It can be seen, by comparing Figures 6 and 10 that for all ratios of exterior over interior Biot moduli up to one, that the thermal shock condition always produces a larger maximum stress on the inside surface than the steady state condition.

By comparing Figures 6 and 11, it can be seen that for a ratio of exterior over interior Biot moduli of one, the steady state stresses always produce a larger maximum stress on the outside surface than the thermal shock condition for inside heating.

Figures 9 and 13 represent the thermal shock and steady state stresses on the outside surface for outside heating. Thus for outside heating, thermal shock produces a larger maximum stress on the outside surface than the steady state condition for a ratio of interior over exterior Biot moduli of one.

Figures 9 and 12 show that for outside heating the steady state condition with an interior over exterior Biot moduli ratio of one produces a larger maximum stress than the thermal shock condition on the inside surface.

Thus a general statement can be made concerning thermal shock and steady state heating with the ratio of the Biot modulus of non-heated surface over the Biot modulus of heated surface equal to one. The thermal shock always produces the largest maximum stress on the heated surface, and the steady state condition always produces the largest maximum stress on the non-heated surface. As the ratio of the Biot moduli changes, by changing the Biot modulus of the non-heated surface, the steady state stresses change, but the thermal shock stresses do not change. The thermal shock stresses do not change because the maximum stress occurs at the time when the non-heated surface just begins to change temperature; thus the Biot modulus of that surface could be any value and not change the result.

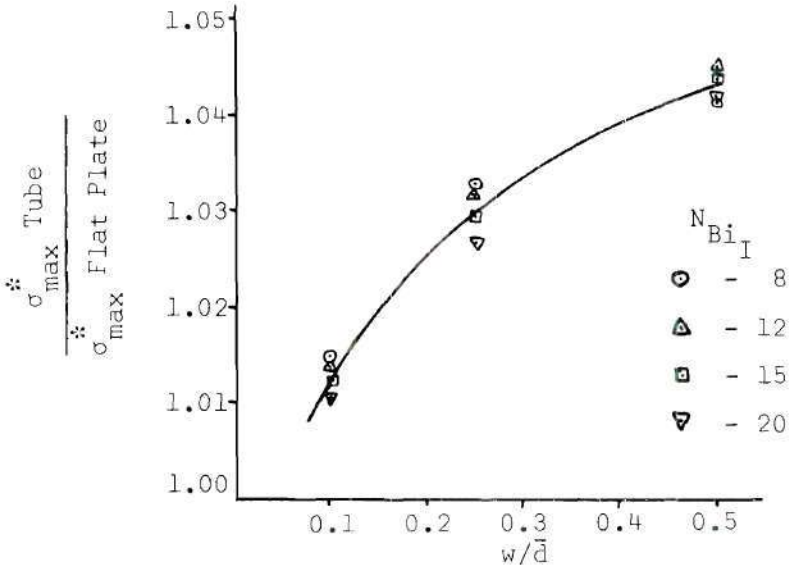

Figure 14. Correction Factor for Inside Heating Thermal Shock of Tubes

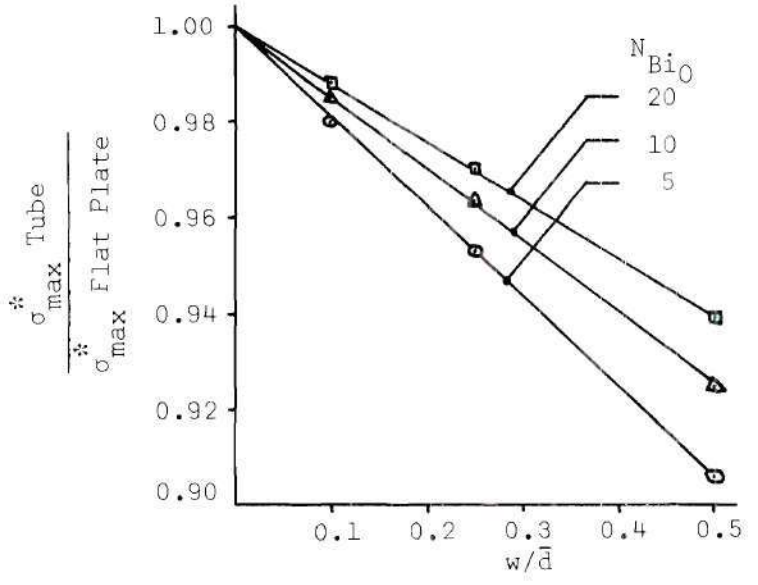

Figure 15. Correction Factor for Outside Heating Thermal Shock of Tubes

APPENDIX A

COMPUTER PROGRAM

The numerical analysis of the temperature and stress distributions were performed on the IBM 360/50 system by a program written in Fortran IV language. The program is presented on the following pages. It should be clear to anyone familiar with the Fortran IV language as the program is fully documented with comment statements. The input data are explained below.

Input Data

Material Properties

EE modulus of elasticity (P.S.I.)

V Poisson's ratio

ALP coefficient of thermal expansion (in/in °F)

KT coefficient of thermal conductivity (BTU/ft °F hr)

CT heat capacity per unit volume (BTU/ft^3 °F)

Tube Dimensions and Heating Parameters

RI inside tube radius (inches)

RO outside tube radius (inches)

TI inside temperature (°F)

TTUBE tube temperature (°F)

TO outside temperature (°F)

BI Biot modulus of inside surface

BO Biot modulus of outside surface

Program Indicators

N number of nodal points

IND1 temperature writing indicator

IND2 stress writing indicator

IND3 number of time increments the temperature is stepped between stress calculations

```
/JOB GO
      DIMENSION R(21),A(21),B(21),C(21),D(21),E(21),
     1SRAD(21),STAN(21),F(21),PHI(21),R1(21)
      DOUBLE PRECISION G(21,22),H,FF1,T(21,151),TT(21)
      REAL KT
C   READ MATERIAL PROPERTIES
      READ(5,5)EE,V,ALP,KT,CT
C   READ TUBE DIMENSIONS AND HEATING PARAMETERS
      READ(5,5)RI,RO,TI,TTUBE,TO,BI,BO
5     FORMAT(7F10.3)
C   READ PROGRAM INDICATORS
6     READ(5,7)N,IND1,IND2,IND3
7     FORMAT(I3)
      HI=BI*KT/((RO-RI)/12)
      HO=BO*KT/((RO-RI)/12)
      DR1=(RO-RI)/(N-1)/12.0
      DR=DR1*12.0
C   THE TIME INCREMENT IS CALCULATED FROM THE SPATIAL INCREMENT
      DT1=CT*DR1**2/6.0/KT
      DT2=CT*DR1**2/(2.*(KT+HI*DR1))
      IF(DT1-DT2)10,9,9
9     DT=DT2
      GO TO 11
10    DT=DT1
11    CONTINUE
      DO 50 I=1,N
      R1(I)=RI/12.0+DR1*(I-1)
50    R(I)=R1(I)*12.0
      WRITE(6,51)
51    FORMAT(10X,'RADII')
110   FORMAT(10F10.2/)
      WRITE(6,110)(R(I),I=1,N)
      DO 710 I=1,N
710   TT(I)=TTUBE
C     START OF NEW TEMPERATURE CYCLE
```

```
712    CONTINUE
       L10=L10+1
713    DO 714 I=1,N
714    T(I,1)=TT(I)
C    CALCULATE TEMPERATURE FOR (IND3) TIME INCREMENTS
715    DO 720 J=1,IND3
       M1=N-1
       DO 730 I=2,M1
730    T(I,J+1)=T(I,J)+KT*DT/CT*((T(I+1,J)-2*T(I,J)+T(I-1,J))/
      1DR1**2+(T(I+1,J)-T(I-1,J))/(2*R1(I)*DR1))
       T(1,J+1)=(2.*HI*DR1*TI+4.*KT*T(2,J+1)-KT*T(3,J+1))
      1/(3.*KT+2.*HI*DR1)
720    T(N,J+1)=(2.*HO*DR1*TO+4.*KT*T(N-1,J+1)-KT*T(N-2,J+1))
      1/(3.*KT+2.*HO*DR1)
       JT=JT+IND3
       TIMEN=JT*DT*KT/CT/((RO-RI)/12)**2
       TIME=JT*DT*3600.0
       WRITE(6,750)TIME,TIMEN
750    FORMAT(10X,'TOTAL TIME=',F7.2,' SECONDS',5X,
      1'NONDIMENSIONAL TIME=',F10.4,/)
       DO 740 I=1,N
740    TT(I)=T(I,IND3+1)
C      THE DIMENSIONS FOR STRESS ARE IN INCHES
       N1=N+1
       N2=N+2
       M1=N-1
       M2=N-2
       M3=N-3
       M4=N-4
       M5=N-5
C      IF IND1=1 WRITE,IND1=2 DO NOT WRITE
       IF(IND1-1)52,52,119
52     WRITE(6,53)
53     FORMAT(10X,'TEMPERATURE')
       WRITE(6,110)(TT(I),I=1,N)
```

```
119   CONTINUE
C     TO GENERATE THE COEFFICIENTS OF THE FINITE DIFFERENCE EQUATIONS
      DO 700 I=2,M1
      I1=I+1
      IM1=I-1
      A(I)=-R(I)**2
      B(I)=(2*R(I)**2)+((2*R(I)+DR)*DR)
      C(I)=-4.*R(I)*DR
      D(I)=(-2*R(I)**2)+((2*R(I)-DR)*DR)
      E(I)=-A(I)
700   F(I)=-EE*(R(I)*DR)**2*ALP*(TT(I1)-TT(IM1))/(1.-V)
      A(N)=3*R(N)**2
      B(N)=-14.*R(N)**2-2.*R(N)*DR
      C(N)=24.*R(N)**2+8.*R(N)*DR-DR**2
      D(N)=-18.*R(N)**2-10.*R(N)*DR+4.*DR**2
      E(N)=5.*R(N)**2+4.*R(N)*DR-3.*DR**2
      F(N)=-EE*ALP*(R(N)*DR)**2*(3.*TT(N)-4.*TT(N-1)+TT(N-2))/(1.-V)
C     TO FORM AN AUGMENTED COEFFICIENT MATRIX
      G(1,1)=1.0
      DO 91 J=2,N1
91    G(1,J)=0.0
      DO 100 I=2,M4
      KM1=I-1
      K=I
      K1=I+1
      K2=I+2
      K3=I+3
      K4=I+4
      K5=I+5
      DO 150 J=1,KM1
150   G(I,J)=0.0
      G(I,K)=A(K2)
      G(I,K1)=B(K2)
      G(I,K2)=C(K2)
      G(I,K3)=D(K2)
```

```
      G(I,K4)=E(K2)
      DO 200 J=K5,N
200   G(I,J)=0.0
100   G(I,N1)=F(K2)
      I=N-3
      DO 250 J=1,M5
250   G(I,J)=0.0
      G(I,M4)=A(N)
      G(I,M3)=B(N)
      G(I,M2)=C(N)
      G(I,M1)=D(N)
      G(I,N)=E(N)
      G(I,N1)=F(N)
      I=N-2
      DO 300 J=1,M4
300   G(I,J)=0.0
      G(I,M3)=A(M1)
      G(I,M2)=B(M1)
      G(I,M1)=C(M1)+E(M1)
      G(I,N)=D(M1)
      G(I,N1)=F(M1)
      I=N-1
      G(I,1)=0.0
      G(I,2)=C(2)+A(2)
      G(I,3)=D(2)
      G(I,4)=E(2)
      DO 350 J=5,N
350   G(I,J)=0.0
      G(I,N1)=F(2)
      I=N
      G(I,1)=0.0
      G(I,2)=B(3)
      G(I,3)=C(3)
      G(I,4)=D(3)
      G(I,5)=E(3)
```

```
      DO 400 J=6,N
400   G(I,J)=0.0
      G(I,N1)=F(3)
C     TO PRODUCE A LEADER OF UNITY IN EACH ROW
      DO 500 I=1,N
      J=0
510   J=J+1
      IF(G(I,J))520,510,520
520   H=G(I,J)
      DO 500 J=1,N1
500   G(I,J)=G(I,J)/H
C     TO PRODUCE A MATRIX WITH ZEROS BELOW THE DIAGONAL
      DO 530 J=1,N1
530   G(M3,J)=G(M3,J)-G(M4,J)
      J=0
540   J=J+1
      IF(G(M3,J))545,540,545
545   H=G(M3,J)
      DO 546 J=1,N1
546   G(M3,J)=G(M3,J)/H
      DO 550 J=1,N1
550   G(M2,J)=G(M2,J)-G(M3,J)
      J=0
560   J=J+1
      IF(G(M2,J))570,560,570
570   H=G(M2,J)
      DO 580 J=1,N1
580   G(M2,J)=G(M2,J)/H
      I=N-1
      L=0
590   J=0
600   J=J+1
      IF(G(I,J))610,600,610
610   M=J
      DO 620 J=1,N1
```

```
620   G(I,J)=G(I,J)-G(M,J)
      J=0
660   J=J+1
      IF(G(I,J))670,660,670
670   H=G(I,J)
      DO 630 J=1,N1
630   G(I,J)=G(I,J)/H
      IF((N-2)-M)640,640,590
640   L=L+1
      I=N
      IF(L-2)590,590,650
650   CONTINUE
C     TO REDUCE THE AUGMENTED MATRIX
      DO 810 J=1,M2
      K=N1-J
      KM1=K-1
      FF1=G(K,N1)
      DO 810 I=2,KM1
      G(I,N1)=G(I,N1)-FF1*G(I,K)
810   G(I,K)=0.0
C     TO GENERATE THE AIRY STRESS FUNCTION
      DO 900 I=1,N
900   PHI(I)=G(I,N1)
C     TO CALCULATE STRESSES FROM THE AIRY STRESS FUNCTION
      SRAD(1)=0.0
      STAN(1)=2.*PHI(2)/DR**2
      SRAD(N)=0.0
      STAN(N)=2.*(PHI(M1)-PHI(N))/DR**2
      DO 910 I=2,M1
      I1=I+1
      IM1=I-1
      SRAD(I)=(PHI(I1)-PHI(IM1))/2./R(I)/DR
910   STAN(I)=(PHI(I1)-2.*PHI(I)+PHI(IM1))/DR**2
      IF(TI-TO)902,902,903
902   DELT=TTUBE-TO
```

```
      GO TO 904
903   DELT=TTUBE-TI
904   STANN1=STAN(1)*(1.0-V)/EE/ALP/DELT
      STANNN=STAN(N)*(1.-V)/EE/ALP/DELT
C     IF IND2=1 WRITE,IND2=2 DO NOT WRITE
      IF(IND2-1)911,911,135
911   WRITE(6,915)
915   FORMAT(/10X,'STRESS FUNCTION')
      WRITE(6,110)(PHI(I),I=1,N)
      WRITE(6,916)
916   FORMAT(/10X,'RADIAL STRESSES')
      WRITE(6,110)(SRAD(I),I=1,N)
      WRITE(6,917)
917   FORMAT(/10X,'TANGENTIAL STRESS')
      WRITE(6,110)(STAN(I),I=1,N)
      GO TO 140
C     IF IND2=1 DO NOT WRITE,IND2=2 WRITE
135   WRITE(6,136)STAN(1),STAN(N),STANN1,STANNN
136   FORMAT(32X,'INSIDE',11X,'OUTSIDE',/5X,'TANGENTIAL STRESS'
     1,6X,F12.3,6X,F12.3,/,5X,'NONDIMENSIONAL STRESS'
     1,2X,F12.5,6X,F12.5/)
140   CONTINUE
      IF(L10-10)712,712,143
143   WRITE(6,8)
8     FORMAT('1')
144   STOP
      END
/DATA
```

APPENDIX B

NONDIMENSIONAL ANALYSIS

The energy equation[1] for an isotropic elastic solid is

$$\nabla(k\nabla T) = \rho c_E \dot{T} - T \frac{\partial \sigma_{ij}}{\partial T} \dot{\epsilon}_{ij} \tag{52}$$

As shown in Reference (1), the coupling term will be small if

$$\frac{\dot{\epsilon}_{kk}}{3\alpha\dot{T}} << 20 \tag{53}$$

The analysis of this thesis is restricted to transient heating conditions where the coupling term is small. With this restriction, the analysis will be conducted subject to later verification that the coupling term is small in the range of the parameters investigated.

Neglecting the coupling term, Equation 52 reduces to the uncoupled heat conduction equation

$$\nabla(k\nabla T) = \rho c\dot{T}$$

where the specific heat at constant strain, C_E, was replaced with the specific heat at constant pressure, C.

In the case of no axial and no tangential heat conduction this equation in polar coordinates reduces to

$$\frac{1}{r}\frac{\partial}{\partial r}\left(kr\frac{\partial T}{\partial r}\right) = \rho c\frac{\partial T}{\partial t}$$

If the thermal conductivity is assumed to be independent of temperature, the above equation reduces to the governing heat conduction equation, Equation 1,

$$\frac{\partial^2 T}{\partial r^2} + \frac{1}{r}\frac{\partial T}{\partial r} = \frac{1}{D}\frac{\partial T}{\partial t} \qquad (1)$$

where $D = k/\rho c$.

Nondimensional Form of Heat Conduction Equation

By the introduction of the following four nondimensional parameters, the heat conduction equation, Equation 1, can be nondimensionalized. The Biot modulus is

$$N_{Bi} = \frac{hw}{k}$$

The Fourier number is

$$N_{Fo} = \frac{Dt}{w^2}$$

The nondimensional radius is

$$r^* = r/w$$

The nondimensional temperature is

$$T^* = \frac{T - T_{initial}}{T_{fluid} - T_{initial}}$$

The nondimensional form of the heat conduction equation, Equation 1, is

$$\frac{\partial^2 T^*}{\partial r^{*2}} + \frac{1}{r^*}\frac{\partial T^*}{\partial r^*} = \frac{\partial T^*}{\partial N_{Fo}} \tag{54}$$

The nondimensional form of the boundary conditions, Equations 3, is

$$\begin{aligned} -\frac{\partial T^*}{\partial r^*} &= N_{Bi_I} \qquad \text{at } r^* = r_I^* \\ \frac{\partial T^*}{\partial r^*} &= N_{Bi_O} \qquad \text{at } r^* = r_O^* \end{aligned} \tag{55}$$

The nondimensional form of the initial condition, Equation 2, is

$$T^* = 0 \qquad \text{for } R_I^* \leq r^* \leq r_O^* \tag{56}$$

Nondimensional Form of the Stress Equations

The solution to the stress problem, as shown in Chapter II, is obtained through the solution of the equilibrium equation, Equation 4, the compatibility equation, Equation 11, and the boundary conditions,

Equations 5. By introducing one additional nondimensional parameter the stress equations can be nondimensionalized. The nondimensional stress is

$$\sigma^* = \frac{\sigma(1-\mu)}{E\alpha(T_{fluid}-T_{initial})} \tag{57}$$

The nondimensional form of the equilibrium equation, Equation 4, is

$$\frac{d\sigma^*_{rr}}{dr^*} + \frac{\sigma^*_{rr} - \sigma^*_{\theta\theta}}{r^*} = 0 \tag{58}$$

The nondimensional form of the compatibility equation, Equation 11, is

$$\frac{d\sigma^*_{\theta\theta}}{dr^*} - \frac{\mu}{1-\mu}\frac{d\sigma^*_{rr}}{dr^*} - \frac{1}{r^*(1-\mu)}(\sigma^*_{rr}-\sigma^*_{\theta\theta}) = -\frac{dT^*}{dr^*} \tag{59}$$

The nondimensional form of the boundary conditions, Equations 5, is

$$\begin{aligned} \sigma^*_{rr} &= 0 \qquad \text{at } r^* = r^*_I \\ \sigma^*_{rr} &= 0 \qquad \text{at } r^* = r^*_O \end{aligned} \tag{60}$$

The solution to the stress equations is obtained by the introduction of the nondimensional stress function, which is defined as

$$\phi^* = \frac{\phi(1-\mu)}{E\alpha\Delta T w^2}$$

The stresses in terms of ϕ^* are

$$\sigma^*_{rr} = \frac{1}{r^*}\frac{d\phi^*}{dr^*}$$

$$\sigma^*_{\theta\theta} = \frac{d^2\phi^*}{dr^{*2}}$$

By substitution it can be seen that this stress function identically satisfies the equilibrium equation, Equation 58. The compatibility equation, Equation 59, in terms of the nondimensional stress function is

$$\frac{d^3\phi^*}{dr^*} + \frac{1}{r^*}\frac{d^2\phi^*}{dr^{*2}} - \frac{1}{r^{*2}}\frac{d\phi^*}{dr^*} = -\frac{dT^*}{dr^*} \tag{61}$$

The nondimensional form of the boundary conditions is

$$\frac{d\phi^*}{dr^*} = 0 \qquad \text{and} \qquad \phi^* = 0 \qquad \text{at } r^* = r^*_I$$

$$\frac{d\phi^*}{dr^*} = 0 \qquad \text{at } r^* = r^*_O \tag{62}$$

Equations 61 and 62 replace Equations 58, 59 and 60, and together with Equations 54, 55 and 56 define the problem. Symbolically, the temperature field is defined through one parameter, N_{Bi}, and can be expressed in terms of two dependent variables, r^* and N_{Fo}:

$$T^*(r^*, N_{Fo}) = f(N_{Bi})$$

The "stress" field is defined by the solution to Equations 61, 62, 54, 55 and 56, and is represented as:

$$\phi^* = g(r^*, N_{fo}, N_{Bi})$$

The nondimensional form of the decoupling equation, Equation 53, becomes

$$\dot{\epsilon}^*_{kk}/\dot{T}^* << 60\alpha(T_{fluid}-T_{initial}) \qquad (63)$$

Verification of Uncoupling Effect

To verify that the uncoupling term is maintained within the limits of Equation 63, the time rate of change of strain and temperature were obtained from an example problem. The example problem is one where the ambient temperature was 1000°F above the initial temperature and the Biot modulus was 20. The numerical computations were carried out for steel with $E\alpha\Delta T/(1-\mu) = 257000.0$. The maximum value for the ratio of strain rate to the time rate of change of temperature, according to the left-hand side of Equation 63 was found to be 1.53×10^{-2}, while Equation 63 would permit the upper limit of 36×10^{-2}. Thus the use of the uncoupled equations did not produce any appreciable error for Biot moduli between 0.5 and 20, and a temperature difference of 1000°F.

BIBLIOGRAPHY

1. Boley, B. A. and Weiner, J. H., *Theory of Thermal Stresses*, John Wiley and Sons, Inc., New York, N.Y., 1960, pp. 31, 42-43.

2. Dusinberre, G. M., *Heat-Transfer Calculations by Finite Differences*, International Textbook Company, Scranton, Pa., 1961, p. 13.

3. Fung, Y. C., *Foundations of Solid Mechanics*, Prentice-Hall, Inc., Englewood Cliffs, N. J., 1965, pp. 389-390.

4. Fox, L., *Two-Point Boundary Problems*, Oxford at the Clarendon Press, Oxford, England, 1957, pp. 138-139.

5. Gatewood, B. E., *Thermal Stresses*, McGraw-Hill Book Company, Inc., New York, N. Y., 1957, passim.

6. Hildebrand, F. B., *Methods of Applied Mathematics*, Prentice-Hall, Inc., Englewood Cliffs, N. J., 1952, passim.

7. Johns, D. J., *Thermal Stress Analysis*, Pergamon Press, Oxford, England, 1965, p. 27.

8. Kreith, F., *Principles of Heat Transfer*, International Textbook Company, Scranton, Pa., 1958, pp. 25-27, 141.

9. Lowan, A. N., *The Operator Approach to Problems of Stability and Convergence of Solutions of Difference Equations*, Scripta Mathematica, New York, N. Y., 1957.

10. Manson, S. S., *Thermal Stress and Low-Cycle Fatigue*, McGraw-Hill Book Company, Inc., New York, N. Y., 1966, pp. 276-283.

11. Parcus, H., *Thermoelasticity*, Blaisdell Publishing Co., Waltham, Mass., 1968, passim.

12. Schneider, P. J., *Conduction Heat Transfer*, Addison-Wesley Publishing Company, Inc., Cambridge, Mass., 1955, pp. 298-302.

13. Shields, P. C., *Elementary Linear Algebra*, Worth Publishers, Inc., New York, N. Y., 1968, passim.

14. Timoshenko, S., and Goodier, J. N., *Theory of Elasticity*, McGraw-Hill Book Company, Inc., New York, N. Y., 1951, passim.